

Velocity correction for Hubble constant measurements from standard sirens

Suvodip Mukherjee^{1,2,3*}, Guilhem Lavaux¹, François R. Bouchet¹, Jens Jasche⁴, Benjamin D. Wandelt^{1,2,5}, Samaya Nissanke³, Florent Leclercq⁶, and Kenta Hotokezaka^{7,8}

¹ Institut d’Astrophysique de Paris (IAP), CNRS & Sorbonne Université, UMR 7095, 98 bis bd Arago, 75014 Paris, France

² Institut Lagrange de Paris (ILP), Sorbonne Universités, 98 bis Boulevard Arago, 75014 Paris, France

³ Gravitation Astroparticule Physics Amsterdam (GRAPPA), Anton Pannoeoek Institute for Astronomy and Institute for High-Energy Physics, University of Amsterdam, Science Park 904, 1090 GL Amsterdam, The Netherlands

⁴ The Oskar Klein Centre, Department of Physics, Stockholm University, AlbaNova University Centre, SE 106 91 Stockholm, Sweden

⁵ Center for Computational Astrophysics, Flatiron Institute, 162 5th Avenue, New York, NY 10010, USA

⁶ Imperial Centre for Inference and Cosmology (ICIC) & Astrophysics Group, Imperial College London, Blackett Laboratory, Prince Consort Road, London SW7 2AZ, United Kingdom

⁷ Department of Astrophysical Sciences, Princeton University, Princeton, NJ, 08540, USA

⁸ Research Center for the Early Universe, Graduate School of Science, University of Tokyo, Bunkyo-ku, Tokyo 113-0033, Japan

November 25, 2020

ABSTRACT

Gravitational wave (GW) sources are an excellent probe of the luminosity distance and offer a novel measure of the Hubble constant, H_0 . This estimation of H_0 from standard sirens requires an accurate estimation of the cosmological redshift of the host galaxy of the GW source, after correcting for its peculiar velocity. Absence of an accurate peculiar velocity correction affects both the precision and accuracy of the measurement of H_0 , particularly for nearby sources. We propose a framework to incorporate such a peculiar velocity correction for GW sources. A first implementation of our method to the event GW170817 combined with the Very Large Baseline Interferometry (VLBI) observation leads to a revised value of $H_0 = 68.3^{+4.6}_{-4.5}$ km s⁻¹ Mpc⁻¹. While this revision is minor, it demonstrates that our method makes it possible for obtaining an unbiased and accurate measurements of H_0 at the precision required for the standard siren cosmology.

Key words. Cosmology: observations—cosmological parameters—Gravitational waves—Galaxies: peculiar

1. Introduction

Attempts to make an accurate measurement of the expansion rate of the Universe at the present epoch, known as Hubble constant (H_0), is ongoing since the discovery of the expanding Universe¹ by Lemaître (1927, 1931) and Hubble (1929). Several complementary approaches measure its value with high precision (Hinshaw et al. 2013; Bennett et al. 2013; Planck collaboration 2014; Anderson et al. 2014; Planck collaboration 2016; Cuesta et al. 2016; Planck collaboration 2018; Riess et al. 2019). However, current measurements of H_0 obtained using standard rulers anchored in the early Universe (Cosmic Microwave Background (CMB), Baryon Acoustic Oscillations (BAO)) (Planck collaboration 2014; Anderson et al. 2014; Aubourg et al. 2015; Planck collaboration 2016; Macaulay et al. 2019) and Big Bang Nucleosynthesis (BBN) (Addison et al. 2018; Abbott et al. 2018) differ from late-Universe probes using standard candles (supernovae (SN) type-Ia) (Reid et al. 2009; Riess et al. 2019), strong lensing from the H0LiCOW project (Wong et al. 2019) and using the angular diameter distance between the lensed images as

a calibrator (Jee et al. 2019). A recent measurement of H_0 from the Carnegie-Chicago Hubble program by using the Tip of the Red Giant Branch (TRGB) as a calibrator for the SN type-Ia reduces the tension (Freedman et al. 2019). However, a more recent analysis by Yuan et al. (2019) has claimed inaccuracies in the calibration of Freedman et al. (2019), which again aggravates the tension.

Taken at face value, this tension, statistically significant by more than 4σ , would necessitate revision of the flat Lambda Cold Dark Matter (Λ CDM) model of cosmology (Verde et al. 2013; Bernal et al. 2016; Di Valentino et al. 2017; Kreisch et al. 2019; Poulin et al. 2019; Lin et al. 2019; Agrawal et al. 2019; Verde et al. 2019; Knox & Millea 2019). Whether this discrepancy is associated with systematic or calibration errors in either of the data sets or indicates new physics is currently a subject of intense debate. In this context, the spotlight has turned to standard sirens (Schutz 1986; Abbott et al. 2017a) with binary neutron star mergers as an independent probe with the potential to reach the required percent-level precision to validate the low redshift (z) determination of H_0 (Dalal et al. 2006; Nissanke et al. 2010; Nissanke et al. 2013a; Chen et al. 2018; Feeny et al. 2019; Seto & Kyutoku 2018; Mortlock et al. 2018). This potential depends crucially on whether the contamination from the peculiar velocity can be corrected at the required accuracy. The estimation of the cosmic velocity field was made in sev-

* s.mukherjee@uva.nl, mukherje@iap.fr

¹ The International Astronomical Union has recently renamed the Hubble law as the Hubble–Lemaître law, in recognition of the pioneering contribution of Lemaître (<https://www.iau.org/news/pressreleases/detail/iau1812/>)

eral studies (Kaiser et al. 1991; Shaya et al. 1992; Hudson 1994; Davis et al. 1996; Branchini et al. 1999; Saunders et al. 2000; Branchini et al. 2001; Nusser et al. 2001; Hudson et al. 2004; Radburn-Smith et al. 2004; Pike & Hudson 2005; Erdoğan et al. 2006; Lavaux & Hudson 2011b; Davis et al. 2011; Ma et al. 2012; Turnbull et al. 2012a). In this paper, we propose a new framework to obtain an unbiased and accurate measurement of H_0 from GW observations. Our method relies on the `BORG` framework, for Bayesian Origin Reconstruction from Galaxies (Jasche & Wandelt 2013; Jasche et al. 2015; Lavaux & Jasche 2016) to reconstruct the cosmic velocity field using the galaxy field observed in the redshift space. This framework is quite different from the methods used by Abbott et al. (2017a), which depends on the linear velocity estimates from Carrick et al. (2015). Along with the complete Bayesian posterior distribution of the velocity field available from the `BORG` framework, it is also useful in capturing the non-linear velocity component (as discussed in Sec. 4), which goes beyond the framework by Carrick et al. (2015). Our method is an alternative way to incorporate the peculiar velocity corrections to the future GW sources in the sky patch of the 2M++ and SDSS-III samples as discussed in Sec. 4. In order to make a reliable estimation of H_0 from GW sources, it is essential to correct for peculiar velocity using multiple independent approaches to minimize the chance of any systematic bias. The proposal made in this work can be included along with other methods such as Carrick et al. (2015), and Springob et al. (2014) for future GW sources.

The paper is organised as follows, in Sec. 2 we discuss the low redshift probes to H_0 using standard candles and standard sirens. In Sec. 3 and Sec. 4 we discuss the effect of peculiar velocity on luminosity distance and redshift, and discuss a framework `BORG` to estimate it from the cosmological observations. In Sec. 5 we discuss the algorithm to incorporate peculiar velocity correction to the host of standard sirens. Finally in Sec. 6 and Sec. 7 respectively, we obtain the revised value of H_0 from the event GW170817 (Abbott et al. 2019a) and discuss the applicability of our method to the future GW events.

2. Low redshift probes of Hubble constant from standard sirens

All direct low z measurements of H_0 depend on measuring the luminosity distance to the source, which is given by

$$d_L = \frac{c(1+z)}{H_0} \int_0^z \frac{dz}{E(z)}, \quad (1)$$

in a homogeneous Friedmann-Lemaître-Robertson-Walker (FLRW) metric when assuming a stationary source and observer. Here c is the speed of light, and $E(z) \equiv H(z)/H_0 = \sqrt{\Omega_m(1+z)^3 + (1-\Omega_m)}$, within the framework of flat Λ CDM (Hinshaw et al. 2013; Bennett et al. 2013; Planck collaboration 2014; Anderson et al. 2014; Planck collaboration 2016; Cuesta et al. 2016; Planck collaboration 2018) with $\Omega_m = \rho_m/\rho_c$ (matter density ρ_m today divided by the critical density $\rho_c = 3H_0^2/8\pi G$). At very low redshift z the Hubble parameter $H(z)$ is nearly constant, this relation simplifies greatly and becomes independent of the background cosmological model

$$d_L = \frac{cz}{H_0}. \quad (2)$$

Gravitational waves (GW) sources provide a new avenue to measure the luminosity distance since as they provide remarkable standard sirens which only assume that the general theory of

relativity be a valid description; they do not require to be ‘standardized’ using other astrophysical sources. Indeed, as pointed out by Schutz (1986), the distance to the GW sources can be measured without a degeneracy with its redshifted chirp mass \mathcal{M}_z , which is related to the physical chirp mass in the source frame by the relation $\mathcal{M}_z = (1+z)\mathcal{M}$. Source frame chirp mass is related to the mass of each of the compact objects, m_1 and m_2 , by the relation $\mathcal{M} = (m_1 m_2)^{3/5}/(m_1 + m_2)^{1/5}$. The GW strain in the frequency domain can be expressed for the two polarization states h_+ , h_\times , by the relation (Hawking & Israel 1987; Cutler & Flanagan 1994; Poisson & Will 1995; Maggiore 2008)

$$\begin{aligned} h_+(f_z) &= \sqrt{\frac{5}{96}} \frac{G^{5/6} \mathcal{M}_z^2 (f_z \mathcal{M}_z)^{-7/6}}{c^{3/2} \pi^{2/3} d_L} (1 + \cos^2(i)) e^{i\phi_z}, \\ h_\times(f_z) &= \sqrt{\frac{5}{96}} \frac{G^{5/6} \mathcal{M}_z^2 (f_z \mathcal{M}_z)^{-7/6}}{c^{3/2} \pi^{2/3} d_L} \cos(i) e^{i\phi_z + i\pi/2}, \end{aligned} \quad (3)$$

where G is the gravitational constant, c is the speed of light, $f_z = f/(1+z)$ redshifted GW frequency, ϕ_z is the phase of the GW signal and $i \equiv \arccos(\hat{L} \cdot \hat{n})$ is the inclination angle of the GW source which is defined as the angle between the unit vector of angular momentum \hat{L} and the line of sight of the source position \hat{n} . The above expression indicates the presence of a degeneracy between d_L and $\cos(i)$ for individual polarization states. However, the polarization states of GW can be measured as they have different dependency on $\cos(i)$ (Holz & Hughes 2005; Dalal et al. 2006; Nissanke et al. 2010; Nissanke et al. 2013a). The measurement of both polarization states of the GW signal requires multiple detectors, with different relative orientation between the arms of the detectors.

Along with the luminosity distance measurement to the standard sirens, a measurement of the Hubble constant also requires an independent measurement of the redshift of the source. Binary neutron star, black hole–neutron star, supermassive binary black hole mergers are all expected to have electromagnetic counterparts. This can lead to the identification of the host galaxy of the GW source and the redshift to the GW source can be estimated from the electromagnetic spectra of the host using spectroscopic (or photometric) measurement by the relation $1+z = \lambda_o/\lambda_e$.² As a result, by using d_L from the GW signal, and z from the electromagnetic spectra, GW sources provide an excellent avenue to measure Hubble constant using Eq. (2).

3. Luminosity distance and redshift in the presence of large scale structure

The luminosity distance to a source and its observed redshift in a homogeneous FLRW Universe is different from the one in presence of cosmic perturbations.³ The presence of perturbations in the matter density leads to temporal and spatial fluctuations in the metric perturbations (through terms involving Φ , $\dot{\Phi}$, $\nabla\Phi$, $\nabla^2\Phi$), which are related to effects such as, but not limited to, the peculiar velocity of the source and of the observer, the gravitational redshift, the integrated Sachs-Wolfe and gravitational lensing (Sasaki 1987; Kolb et al. 2005; Barausse et al. 2005; Bonvin et al. 2006).

The observed redshift to the source also differs from the cosmological redshift due to the contributions from the difference in the peculiar velocity between the observer v_o and the source

² λ_o and λ_e are the measured and emitted wavelength of the light respectively.

³ The perturbation in the homogeneous FLRW metric is caused by the presence of structures in the Universe.

v_s and also to the gravitational redshift. At low redshift, the most important contributions arise from the difference in the velocity of the observer and source. The observed redshift z_{obs} can be written in terms of the peculiar velocity $v_p = (\mathbf{v}_s - \mathbf{v}_o) \cdot \hat{u}$ ⁴ by the relation $(1 + z_{obs}) = (1 + z) \left(1 + \frac{v_p}{c}\right)$. The corresponding modification in Eq. (2) is

$$d_L = \frac{cz + v_p}{H_0}. \quad (4)$$

This implies that the contribution from the peculiar velocity leads to a bias in the inferred value of H_0 , if not accounted for. For multiple sources with uncorrelated velocities, the effect of ignoring the peculiar velocity component in the average is to produce excess variance in the measurement of H_0 . If we assume the distribution of the peculiar velocity field to be Gaussian with a variance σ_v^2 , then the corresponding excess variance in the H_0 measurement for a source at distance d_L becomes σ_v^2/d_L^2 . The current frameworks to obtain H_0 from the standard sirens use a Gaussian prior on the peculiar velocity (Abbott et al. 2017a; Chen et al. 2018; Feeney et al. 2019). We propose an algorithm to correct for the peculiar velocity contribution to standard sirens.

The peculiar velocity of a host galaxy, $v_p = v_h + v_{vir}$, can arise from two components namely (i) the motion of the halo due to the spatial gradient in the gravitational potential v_h , and (ii) the virial velocity component v_{vir} of the host galaxy inside the halo. The non-rotational velocity component of v_l can be obtained from linear perturbation theory as

$$v_l(\mathbf{x}, z) = -\frac{2}{3} \frac{g(z)}{aH(z)\Omega_m(z)} \nabla_x \Phi, \quad (5)$$

where Φ is the gravitational potential, g is the growth rate related to the linear growth factor D by the relation $g = d \ln D / d \ln a$ and $a = 1/(1+z)$ is the scale factor. At small scales, non-linear effects can be quite important and the previous relation becomes inaccurate. The virial velocity component, v_{vir} , can be related to the mass of the halo, M_h , and the distance to halo center, r , by the relation $v_{vir}^2 \propto M_h/r$, which holds for a virialized system. For a system with a constant mass density, the halo mass and r are related by $M_h \propto r^3$. As a result, the virial velocity v_{vir} is only related to the mass of the halo by the relation $v_{vir}^2 \propto M_h^{2/3}$. This relation indicates that a galaxy with a heavier halo has a larger velocity dispersion than if it resides in a smaller halo. We use the following form, fitted to simulations, to estimate the velocity dispersion of the non-linear velocity component (Sheth & Diaferio 2001)

$$\sigma_{vir} = 476 g_v (\Delta_{nl}(z)E(z)^2)^{1/6} (M_h/10^{15} M_\odot h^{-1})^{1/3}, \quad (6)$$

where $g_v = 0.9$, $\Delta_{nl}(z) = 18\pi^2 + 60x - 32x^2$, and $x = \Omega_m(1+z)^3/E^2(z) - 1$.

4. Estimation of the velocity field using BORG

The velocity field that we use in this work is produced by the ‘‘Bayesian Origin Reconstruction from Galaxies’’ (BORG) probabilistic model of large scale structure, as currently applied to the 2M++ compilation (Lavaux & Hudson 2011a; Jasche & Lavaux 2019) and the SDSS-III/BOSS survey⁵ (Eisenstein et al. 2011; Dawson et al. 2013; Lavaux et al. 2019). The BORG algorithm aims at inferring a fully probabilistic and physically

plausible model of the three-dimensional cosmic matter distribution from observed galaxies in cosmological surveys (see e.g. Jasche & Wandelt 2013; Jasche et al. 2015; Lavaux & Jasche 2016). To that effect, the method solves a large-scale Bayesian inverse problem by fitting a dynamical structure formation model to data and inferring the primordial initial conditions from which presently-observed structures formed. The BORG forward modelling approach marginalizes automatically over unknown galaxy bias, and accounts for selection and evolutionary effects. The variant of BORG that we use for the 2M++ catalogue models the galaxy to dark matter bias using a 3-parameter function motivated by the analysis of N -body simulations (Neyrinck et al. 2014). We note that this bias relation is a local non-linear relation for which conventional understanding of bias on large scale does not apply. It is more akin to a halo occupation distribution for high luminosity. The data specifically selects that behavior as can be seen in Section 5.1 of Jasche & Lavaux (2019). The reader should approach with caution any naive numerical comparison of BORG bias parameters to linear bias values found in the literature. Instead of the linear perturbation result in the previous section, BORG uses a full particle-mesh N -body solver to evolve the initial conditions to a dark matter density distribution at $z \approx 0$ (Jasche & Lavaux 2019) through direct integration of the Hamiltonian dynamics equation.

The BORG model provides a set of points in the parameter space (dimensionality $\approx 256^3$, for initial conditions, and a few more for additional bias parameters) that provides a numerical approximation of the posterior distribution of those parameters given the 2M++ observed galaxy distribution. Once initial and final positions of dark matter particles are known, the velocity field is estimated using the Simplex-in-Cell estimator (SIC, Hahn et al. 2015; Leclercq et al. 2017). The SIC estimator relies on a phase-space interpolation technique, which provides an accurate estimate of velocity fields without the need for commonly used but arbitrary kernel smoothing procedures, such as cloud-in-cell (CIC). It provides a physical picture for velocity fields even in low-density regions, which are poorly-sampled by dark matter particles, and takes into account the multi-valued nature of the velocity field in shell-crossed regions by proper stream averaging.

4.1. Validation of the BORG reconstruction algorithm

In this section, we discuss several validation tests of the BORG velocity field inference. In Section 4.1.1, we assess the validity on the sole basis of the statistics of the reconstructed samples. In Section 4.1.2, we run a BORG analysis on a set of mock tracers to check the unbiasedness and the typical reconstruction errors.

4.1.1. Comparisons to performance of linear perturbation theory

Carrick et al. (2015) is commonly used for correcting the estimated cosmological redshift of observed objects in the Nearby Universe. This model relies on computing the inverse Laplacian operator on a luminosity weighed distribution of the 2M++ galaxies. This model has been fitted to observed distances of galaxies derived from the SFI++ (Springob et al. 2007) and the First Amendment A1 SNIa data (Turnbull et al. 2012b). The BORG model goes beyond this approach. It is based on deriving a physically meaningful velocity field, beyond linear perturbation theory, based on several pieces of information, including the same 2M++ data-set and cosmology.

The performance and need of going beyond linear perturbations has been extensively discussed in the past. The differ-

⁴ The line of sight vector \hat{u} is directed from the observer to the source, i.e., $v \cdot \hat{u} \geq 0$ implies that the source is moving away from the observer.

⁵ SDSS-III/BOSS is the Baryon Oscillation Spectroscopic Survey.

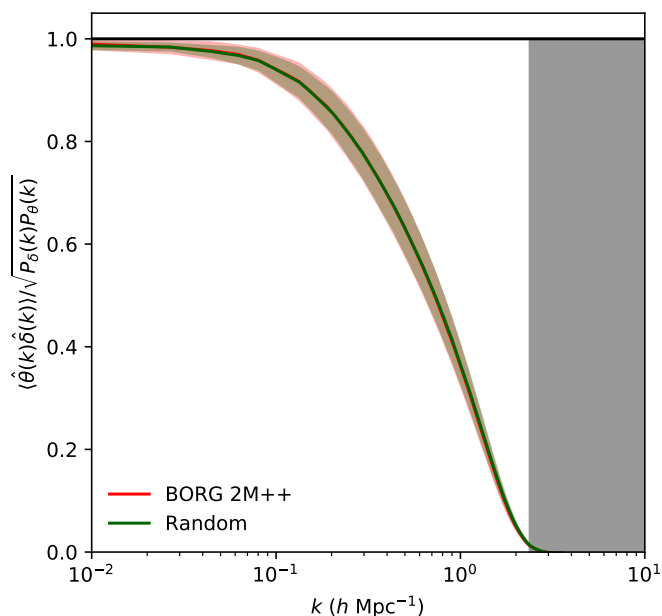


Fig. 1: We show the correlation coefficient between the non-linear density and the negative divergence of the non-linear velocity field, $\theta \equiv -\nabla \cdot \mathbf{v}$. The red line is the ensemble average over the posterior distribution of the cross-correlation and the shaded dark red area is the one standard deviation according to the mean of that cross-correlation derived from the same distribution obtained by **BORG**. The green and shaded green region is the result of computing that same quantities on 80 random realizations. Apart from very minor differences, the two curves are on top of each other, which can be expected as the physical model is the same in both cases. The vertical grey band on the right side indicate the resolution limit of the **BORG** reconstruction. The correlation reach asymptotically one for the largest scales (small k values). The red line is reaching a value of 99% for the largest probed mode. As expected, this cross-correlation goes to zero at small scales (high k value).

ences between the density and velocity power spectra have already been computed analytically on large scales (Scoccimarro 2004) and observed in simulations (Chodorowski & Cielieglag 2002; Scoccimarro 2004; Jennings et al. 2011; Jennings 2012), but they are challenging to derive from observational data. This additionally motivates the **BORG** approach. Leclercq et al. (2015, figure 1) has shown that **BORG**'s constrained simulations of the density field are statistically consistent with independent random realizations. We further emphasize this point here by analyzing the capability of going beyond the linear level for the velocity field. In that respect, we show the cross-correlation between the density and $\theta = -\nabla \cdot \mathbf{v}$ in Figure 1 for constrained realizations and for random simulations generated using the same particle mesh implementation and cosmological setup. There are no visible differences between the cross-correlations between the inferred 2M++ fields and the ones for random realizations. This provides evidence that the density de-correlates from the velocity divergence in the way that is expected from the non-linear gravitational clustering physics of dark matter. We also show in Figure 2 the contribution of the different scales to the total variance of the velocity field. We note that pure Eulerian linear perturbation theory (solid blue line) is systematically above the curve obtained from constrained 2M++ realizations (shades

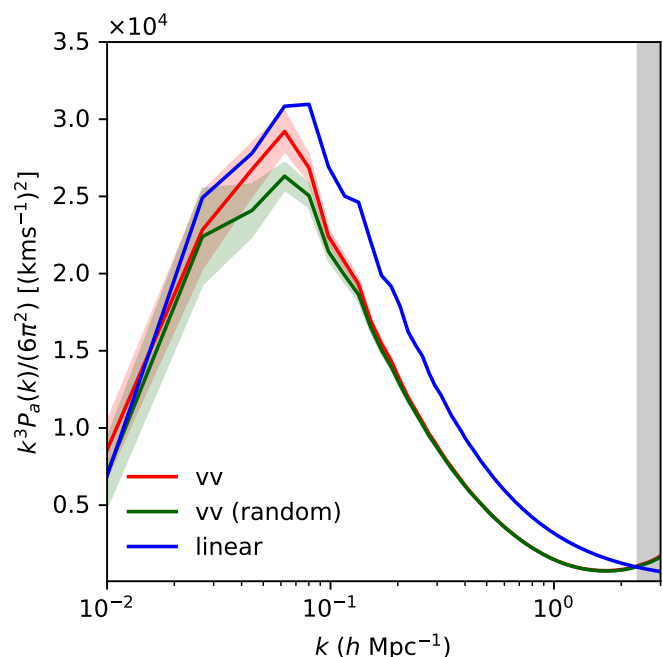


Fig. 2: We show here the ensemble average power-spectrum of the non-linear velocity field scaled, alongside with one standard deviation contour in shaded area. The line and shaded region in red is computed from the ensemble posterior distribution built from the 2M++ data. The line and shaded region in green are measured from 80 random realizations of a Λ CDM universe of the same size. Those random realizations were computed using the same N -body solver, but starting from a random sample of a Gaussian distribution with power-spectrum provided by the Λ CDM model. We show in thick blue line the power spectrum assuming linear theory. We note that large scales are unaffected by non-linearities. Intermediate scales ($k \gtrsim 0.1h \text{ Mpc}^{-1}$, corresponding to $\sim 60h^{-1} \text{ Mpc}$) get non-negligible contributions from non-linear dynamics, as highlighted by the area under the curve. The vertical grey band on the right side indicate the resolution limit of the **BORG** reconstruction ($\sim 2.6h^{-1} \text{ Mpc}$).

of red) and the random velocity field power spectrum (shades of green) for the range of scales of interest. That behaviour of course changes on smaller scales for which random motions become significant, as is hinted by the crossing of the two curves at $k \simeq 2h \text{ Mpc}^{-1}$. For the scales $k < 0.8h \text{ Mpc}^{-1}$, the 2M++ constrained realization matches well with the pure Eulerian linear perturbation theory within the expected variance (denoted in the red shaded region). The drop of power at that scale for the mock and constrained realizations is related to the observation on non-linearities in the power spectrum as pointed out in Jennings et al. (2011).

The two above points show the limits of using the density field as a predictor for the velocity field on intermediate scales. It is likely that the linear model may have reached its maximum capacity of prediction.

The **BORG** derived non-linear model of the velocity field is physically more realistic; but the simpler model in Carrick et al. (2015) has the virtue of having been compared to distance observations. We intend to do the same in a forthcoming publication for **BORG**. **BORG** is also self-consistently models redshift-space

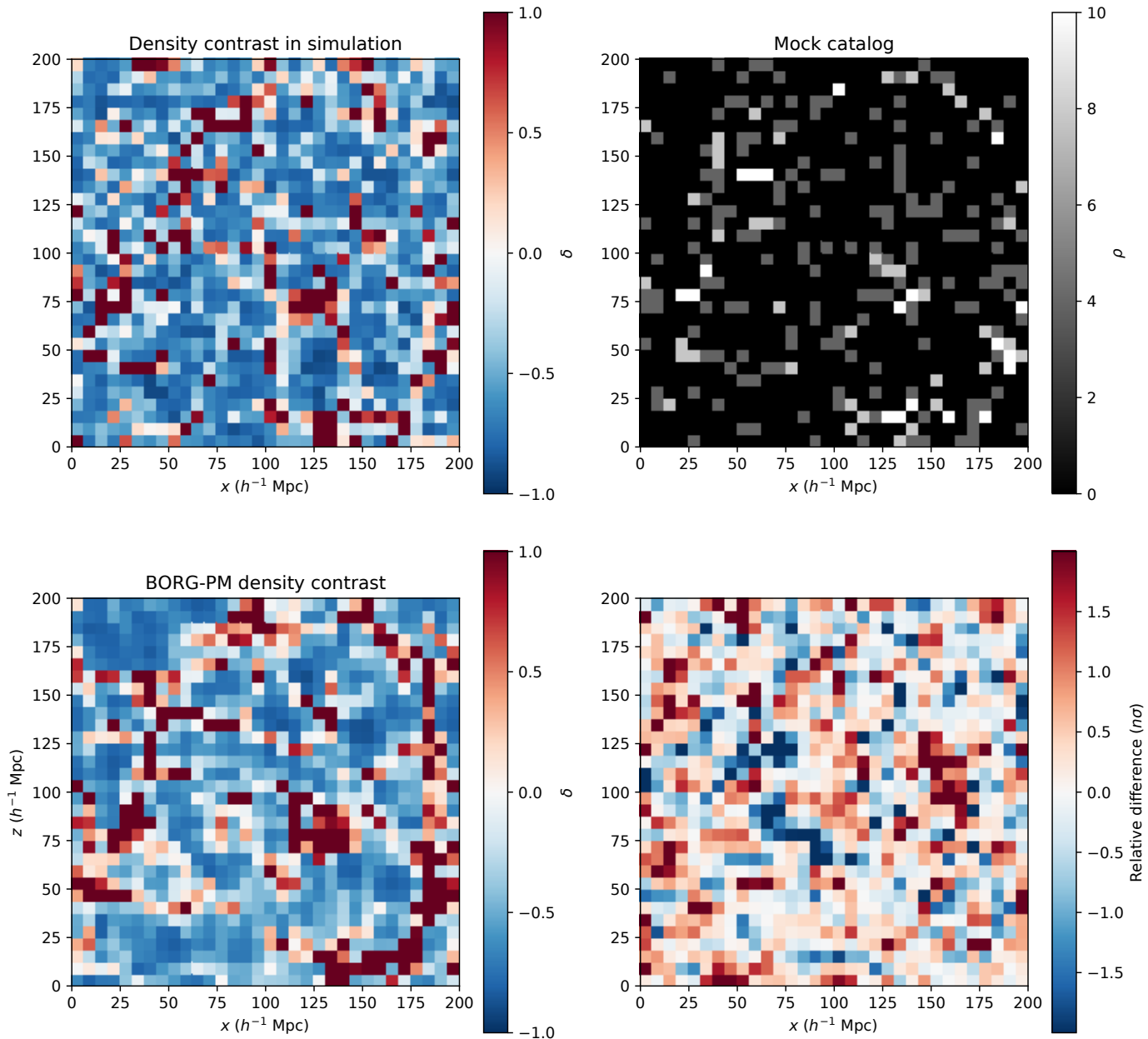


Fig. 3: Tests of the BORG algorithm on a N -body simulation. *Top-left panel*: center slice of the density contrast computed at a resolution of 32^3 from the N -body cosmological simulation used in our test. The simulation itself is obtained with 256^3 dark matter particles with Λ CDM cosmology as used in Jasche & Lavaux (2019). *Top-right panel*: Central slice of grid obtained by assigning objects of the mock catalog to a 32^3 grid with a nearest grid point filter. *Bottom-left panel*: Density slice computed from one posterior sample obtained by BORG. We note the clear spatial correlations between the density field of the fiducial simulation and the inferred sample, despite the very low sampling rate of the mock catalog. *Bottom-right panel*: Difference between the BORG reconstruction and the simulation truth divided by the standard deviation per voxel estimated from the posterior distribution. The BORG posterior covers the truth and gives a conservative estimate of the uncertainty.

distortions, which brings additional information to disentangle galaxy bias from dark matter clustering.

4.1.2. Tests with an N -body simulation

Though a full mock catalog analysis is beyond the scope of this article, we have run some tests on N -body simulations to showcase the correctness of the BORG reconstruction algorithm. Using Gadget-2 (Springel 2005), we have generated an N -body simulation covering a cubic volume with a side length of $200h^{-1}$ Mpc, and sampled with 256^3 particles. We have used

the same cosmology as the one that was used for the BORG 2M++ reconstruction in Jasche & Lavaux (2019). To simplify the test case, we have generated a mock catalog of 8 457 objects directly from the particles of the simulation. The corresponding number density is $\sim 8 - 10$ times smaller than in the observational data. We have then run a BORG-PM reconstruction with 20 time-steps from $z = 50$ to $z = 0$ linearly distributed according to the scale factor, with a grid of 32^3 elements to represent initial conditions. This corresponds to a spatial resolution of $6.25h^{-1}$ Mpc, which

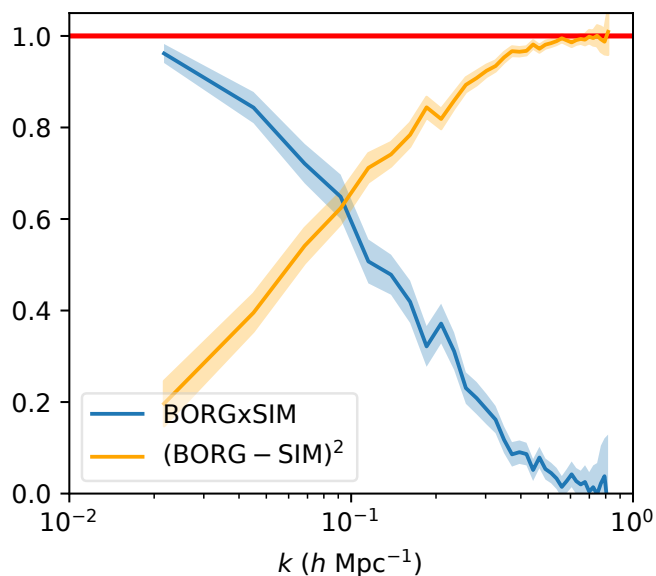


Fig. 4: We show the correlation (blue color) and error residual (orange) for the density field inferred by BORG compared to the simulation density field. We have computed the mean and one standard deviation using the posterior distribution sampled by the BORG chain. Both curves are normalized by the power spectrum of each field. We see that indeed when correlation is weak, we get the maximum relative variance.

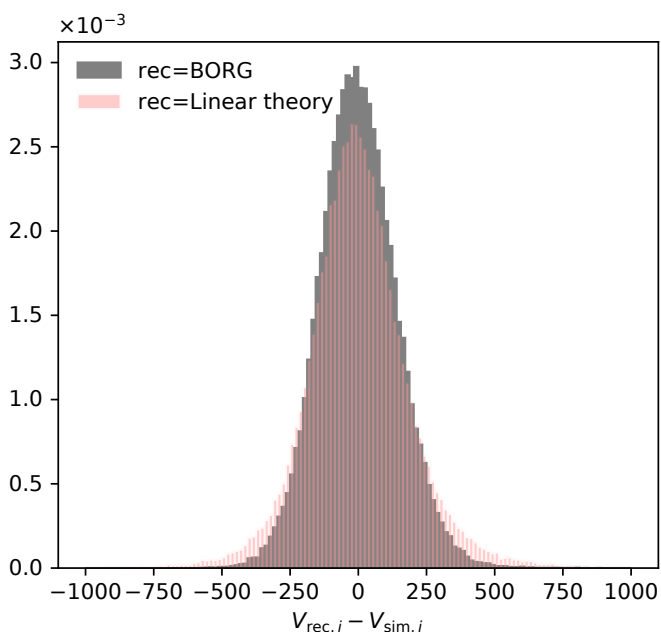


Fig. 5: Tests of the BORG-PM algorithm on a N -body simulation: result for velocity field. We compute the velocity field using the Simplex-In-Cell algorithm using the entire set of particles of the N -body simulation and a resimulation from a single BORG sample. We compute the linear theory prediction for the velocity field based on the mock catalog as well. We show here the residual between each of the reconstructed velocity field and the one of the simulation. The difference is computed for each mesh element. We note that the residual distribution is narrower and have less heavy tails for the BORG reconstruction than for the linear theory one. In both cases, the velocity field is unbiased.

is two to three times lower than the one used for the run on observations.

We show in Figure 3 a slice of the density field of the N -body simulation used for the test (top-left panel), as well as the result of the nearest-grid point assignment of the objects of the mock catalog in that same slice (top-right panel). We also show the density contrasts (bottom-left panel) computed from a single BORG sample, after the burn-in phase. We conclude with a difference plot highlighting the difference between the density field shown in the top-left panel and the bottom-left panel. We note the qualitative agreement between that sample and the density contrasts of the full simulation. In Figure 4, we give a quantitative comparison derived from the entire posterior distribution. The assessment is done by computing the cross-correlation between the BORG density field and the simulation density field and the variance between those two fields. They show that the BORG density field is unbiased and tightly correlated on large scales.

Figure 5 illustrates the distribution of the differences between the velocity field of the simulation and the one provided by BORG inference. The comparison is done for a single sample obtained by BORG and for linear theory directly from the density contrast obtained from the mock catalog (linear theory). The velocity fields are computed using the Simplex-In-Cell algorithm at high resolution and downgraded at 32^3 using local averages. In both cases, the reconstructions are unbiased but linear theory exhibits heavier tails for the residuals, leading to a typical width of 200 km s^{-1} . On the other hand, BORG has residuals with a typical width of 139 km s^{-1} . To further check the unbiasedness, this time using the mock tracers themselves, we show in Figure 6 how the reconstructed velocities, which are obtained through the BORG velocity field, compares to the original mock tracer velocities directly taken from the N -body simulations. The first three panels (top-left, top-right, lower-left) give the scatter plots for each component of the velocities for each mock tracer. The lower-left panel shows the histogram of the residual velocities for the three components together.

We conclude from this test that the peculiar velocities reconstructed with the BORG algorithm are unbiased. They also have typically smaller errors compared to velocities derived using a linear perturbation theory approach.

4.2. Implementation of BORG on 2M++

In Figure 7 (left panel), we show the velocity field in supergalactic coordinates for 2M++ along with the starred spatial position of NGC 4993. The middle panel in Figure 7 indicates the estimate of the velocity field from 2M++ in the Supergalactic coordinate system. Additionally, we further show in the right panel the velocity field as inferred from the SDSS-III/BOSS survey. The latter uses a simpler dynamical model based on first order Lagrangian perturbation theory (Lavaux et al. 2019). The contribution of the non-linear velocity component captured by BORG is shown in Figure 8. This non-linear velocity component is the one captured by the particle mesh solver of BORG, although it is not yet sufficient to resolve virial motions in large scale structures. We denote this regime by "NL" for non-linear. It corresponds to the intermediate "gray" regime when a linear modeling of the velocity field is not sufficient while still not describable without a full non-perturbative description of the non-linear dynamics. To assess its importance we consider two residuals. The left panel shows the relative contribution of the pure NL velocity from BORG with respect to the total velocity contribution by evaluating the expression $|(v_{r,\text{BORG}} - v_{r,\text{linear}})/v_{r,\text{BORG}}|$. It is derived from the difference between the total contribution and the velocity field derived from the gradient of the gravitational potential of

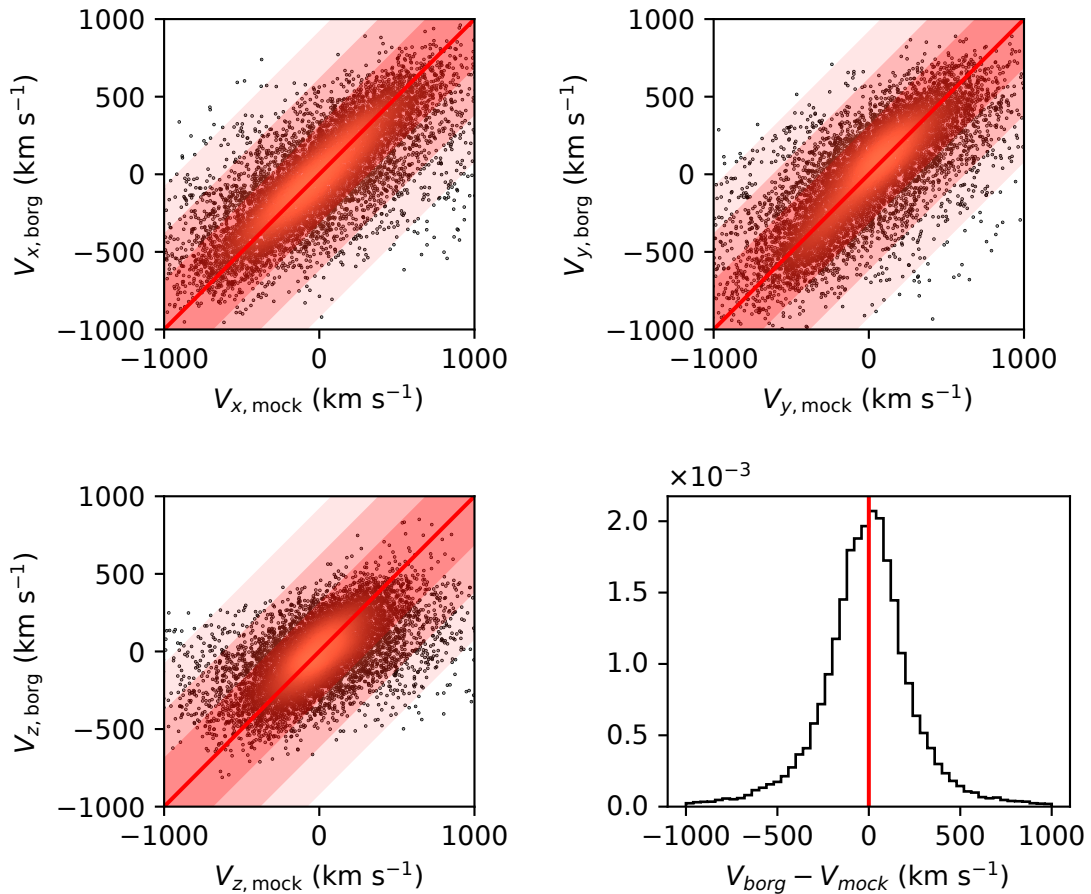


Fig. 6: We show here the components (x top-left, y top-right, z bottom left) of the velocities of the mock tracers as reconstructed from a single sample from `BORG` and compared to the ones provided by the original N -body simulation. The points are color coded according to their local density in the scatter plot to allow a better identification of the central part and the tails of the distribution. The diagonal red line is added for reference and to indicate unbiased velocity reconstruction. The lower right panel shows the histogram of the difference between the `BORG` reconstructed velocities and the original velocities of the mock tracers, for the three components.

the matter density field. We note that the difference between the two fields may originate from at least two reasons: either the linear theory approximation underestimates the amplitude of flow in infalling regions, or it unphysically overestimates the velocity flow close to the peak of the matter density contrast. The right panel shows the estimated standard deviation of the non-linear velocity field, both the total velocity and the residue obtained by taking the difference between the total non-linear and the linear component of the velocity field. This quantity corresponds to the second moment of the probability density function, conditioned on δ_m . We note that this moment does not correspond to the full marginal distribution, and thus it is possible that the conditional standard deviation is reduced compared to the marginal standard deviation. We compute this standard deviation from each bin of matter density field. We note that the ratio of these two standard deviations of the total velocity field and the non-linear component component of the velocity field can go up to $\sim (20-30)\%$ at $\delta_m \sim 4$, indicating that the non-linear component is far from being negligible.

We point that the velocity and density field inference is largely independent of the Hubble constant. Our working coordinate system is using the arbitrary value of $H_0 = 100 \text{ km s}^{-1} \text{ Mpc}^{-1}$. In this coordinate system, the value of H_0 is

irrelevant for computing the dynamics and the observable in the observer coordinate frame. However, what matters is the redshift evolution of $E(z)$, which only depends on relative expansion history. For the portion of Universe that is considered here, the only relevant parameters are $\Omega_m = 0.315$ and $\Omega_\Lambda = 0.685$ (Planck collaboration 2018). The only place where the absolute value of H_0 enters is in the a-priori power spectrum of primordial fluctuations that was used to run the analysis. This is however at least a second-order effect as this only governs the way `BORG` has to fill the missing information in the data space, but not the actual mass distribution that is inferred on large scales.

5. Algorithm for the peculiar velocity correction for standard sirens

The observed GW signal from a network of GW detectors is a probe of the distance to the source as discussed previously. The GW signal parameters comprise the source parameters (such as the chirp mass, individual masses of the compact objects, spin of the individual compact objects, the object's tidal deformability) and parameters that relate to the observer of the GW source such as the luminosity distance d_L , sky location \hat{n} , polarization angle ψ , and the inclination angle i . It is this latter set that is useful

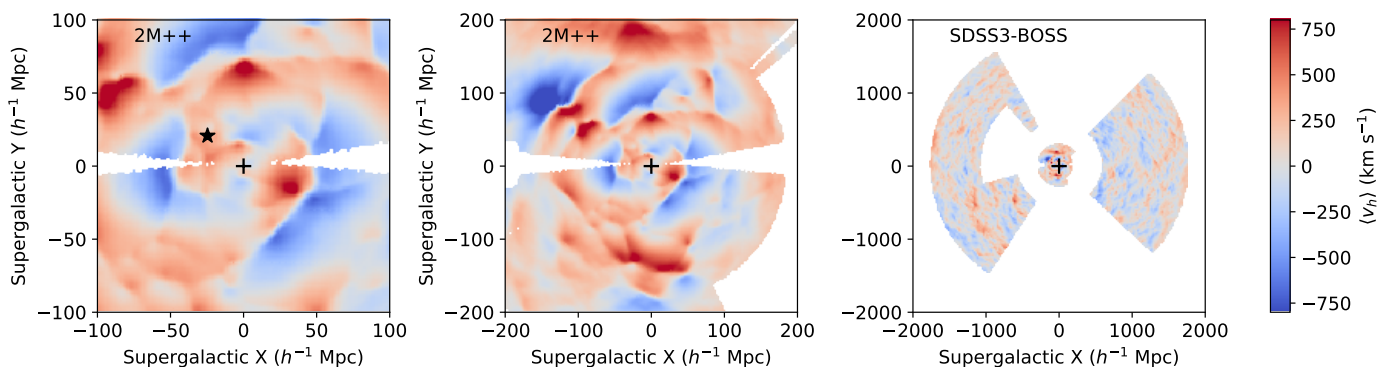


Fig. 7: Global properties of the velocity field that is available from the **BORG** inference framework applied on the 2M++ compilation and on the SDSS-III/BOSS sample of galaxies. The black cross gives the position of the observer. Left panel: velocity field derived from **BORG** in the Supergalactic plane. The black star indicates the spatial position of NGC 4993 which is the host of GW170817. Middle panel: Spatial distribution of the available model of the velocity field in the Supergalactic plane $B=0^\circ$ for the volume of 2M++. Right panel: Same as middle panel but for the SDSS-III/BOSS survey. The part at the center is the region from 2M++.

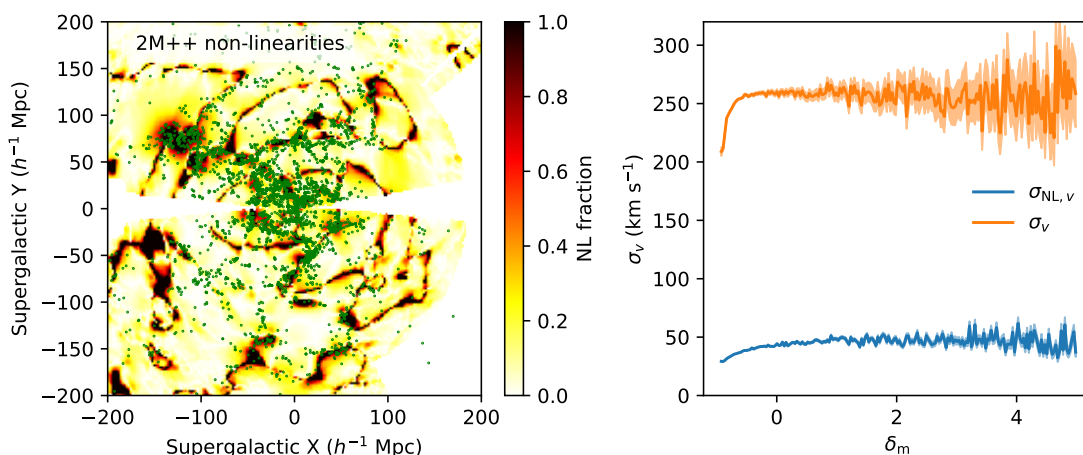


Fig. 8: Non-linearities (NL) modelled by the **BORG** dynamical model. Left panel: the relative difference between the velocity field derived from the gravity field assuming linearity and the non-linear velocity field produced by **BORG** with respect to the total for the ensemble mean fields. Right panel: standard deviation of the velocity field for each density bin (orange curve), and standard deviation of the non-linear velocity, $(v_{r,\text{BORG}} - v_{r,\text{linear}})$, for each density bin (blue curve). We see here that the non-virial, non-linear component of the velocity field can represent a substantial portion of the cosmic velocity field: up to $\sim 25\%$ of the standard deviation of the total velocity field when the local matter density exceeds $\delta_m \gtrsim 4$.

to estimate the value of H_0 (Dalal et al. 2006; Nissanke et al. 2010; Abbott et al. 2017a). The GW strain h_+ and h_\times provides estimates of the luminosity distance and the inclination angle of the GW source. The sky location of the GW source is obtained using the arrival times of the GW signal at different detectors, as well as their antenna function (Fairhurst 2009; Nissanke et al. 2011; Fairhurst 2011; Schutz 2011; Veitch et al. 2012; Nissanke et al. 2013b). The redshift of the GW source may be measured by identifying the host galaxy using the electromagnetic counterpart from the GW sources.

We propose to estimate the peculiar velocity of the host galaxy by estimating the large scale flow v_h from **BORG**, and the small scale motion as a stochastic velocity dispersion using the fitting form given in Eq. (6). We note that v_h is itself composed of the velocity field at the linear order in perturbation, with an additional at least 30% correction from non-linear evolution provided by **BORG** for density $\delta_m > 0$. Using the location of the identified host galaxy (from the electromagnetic counterpart), we estimate the corresponding posterior Probability Density Function (*pdf*)

of the velocity field component v_h from 118 realizations of **BORG** for this galaxy. The virial velocity component is estimated using the mass of the galaxy halo in Eq. (6). The *pdf* of the non-linear velocity field v_{vir} is assumed to be Gaussian distributed. The combined posterior of the peculiar velocity $v_p = v_h + v_{vir}$ can be obtained by convolving the **BORG** posterior of v_h with the *pdf* of v_{vir} .

By combining the measurements from GW data, d_{GW} , the redshift of the host galaxy, \hat{z} , and the peculiar velocity estimate, v_p , and luminosity distance d_L , we can obtain the posterior of H_0 for \mathbf{n} GW sources by using the Bayesian framework

$$P(H_0 | \{d_{GW}\}, \{\hat{z}\}) \propto \prod_{i=1}^{\mathbf{n}} \int dd_L^i dv_p^i \mathcal{L}(d_L^i | H_0, v_p^i, z_i, \hat{\mathbf{u}}_i, d_{GW}^i) \times \mathcal{P}(z_i | \hat{\mathbf{u}}_i) \mathcal{P}(v_p^i | M, \hat{\mathbf{u}}_i) \Pi(H_0), \quad (7)$$

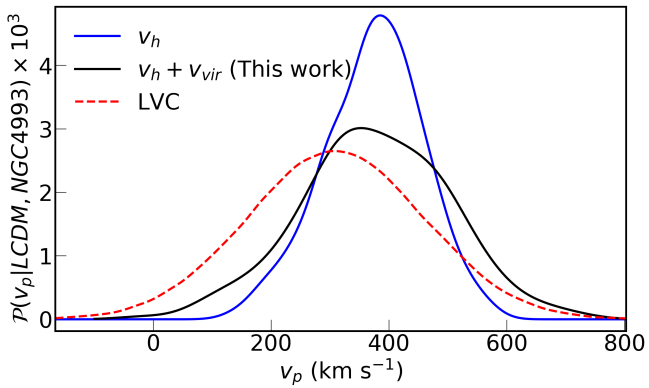


Fig. 9: The posterior of the peculiar velocity of NGC 4993. The blue curve displays the large scale flow, v_p , inferred from BORG while the black curve gives the required total velocity including the virial component within the halo. The posterior of the velocity used by the LIGO Scientific Collaboration and Virgo Collaboration (LVC) is shown with red dashes.

where $\hat{\mathbf{u}}_i(\text{RA}_i, \text{Dec}_i)$ is the sky position,⁶ \mathcal{L} denotes the likelihood which is assumed to be Gaussian, $\mathcal{P}(z_i|\hat{\mathbf{u}}_i)$ is the posterior of the redshift estimate at the GW source $\hat{\mathbf{u}}_i$, $\mathcal{P}(v_p^i|M, \hat{\mathbf{u}}_i)$ is the peculiar velocity estimate using the cosmological method, and $\Pi(H_0)$ is the prior on the value of H_0 .

6. Applying our method to GW170817

6.1. Peculiar velocity estimate for NGC 4993

NGC 4993 is the host galaxy of the event GW170817 (the merger of two neutron stars) which was discovered by the LIGO Scientific Collaboration and Virgo Collaboration (LVC) (Abbott et al. 2017b,a). The distance to the GW170817 inferred from the GW observation is $d_L = 43.8^{+2.9}_{-6.9}$ Mpc (Abbott et al. 2017b,a) and recession velocity of its host NGC 4993 with respect to the CMB rest frame is 3327 ± 72 km s⁻¹ (Abbott et al. 2017a; Crook et al. 2007). The velocity estimate for NGC 4993 has two components, v_h and v_{vir} . We estimate the v_h component from BORG, and the non-linear part of the velocity is obtained using the form mentioned in Eq. (6). NGC 4993 has a halo of mass about $M_h \sim 10^{12} M_\odot$ (Pan et al. 2017; Ebrova & Bilek 2018). The corresponding estimate of σ_{vir} is about 100 km s⁻¹. The excess velocity component is included as an additional velocity dispersion assuming a Gaussian *pdf* of variance σ_{vir}^2 with a zero mean.

The posterior of the peculiar velocity from BORG is shown in blue color in Figure 9 for the Planck-2015 best-fit cosmological parameters (Planck collaboration 2016). The *pdf* of the velocity field is non-Gaussian. The mean value of the velocity field is $\bar{v}_p = 373$ km s⁻¹, and the maximum a posterior value of the velocity field is $v_p^{MP} = 385$ km s⁻¹. The standard deviation of the velocity *pdf* is $\sigma_h \sim 82$ km s⁻¹. The total standard deviation of the velocity due to both v_h and v_{vir} is $\sigma_t = \sqrt{\sigma_h^2 + \sigma_{\text{vir}}^2} \sim 130$ km s⁻¹. The corresponding *pdf* for v_p is shown by the curve in black color in Figure 9. The inferred value of the peculiar velocity of NGC 4993 differs from the value assumed by LVC (Abbott et al. 2017a). Abbott et al. (2017a) considered a velocity distribution which was Gaussian with a mean

and standard deviation given by 310 km s⁻¹ and 150 km s⁻¹ respectively. The estimates of the velocity from our method predict a 24% higher mean value of the velocity and about 13% less standard deviation. The comparison of the distribution of the peculiar velocity between the LVC and our method is shown in red and black respectively in Figure 9.

6.2. Revised H_0 from GW170817

Using our new, more precise estimate of the peculiar velocity for the NGC 4993, we obtain the revised value of H_0 using the Bayesian framework mentioned in Eq. (7) from the data of luminosity distance and inclination angle assuming either a high-spin or a low-spin prior on each compact object (Abbott et al. 2019a). Figure 10 shows the corresponding posterior of H_0 . The posterior of H_0 peaks at $H_0 = 68.3$ km s⁻¹ Mpc⁻¹, instead of 70^{+12}_{-8} km s⁻¹ Mpc⁻¹ from the results of LVC (Abbott et al. 2017a) with the same 68.3% credible interval as obtained by LVC. The marginal difference in the shape of the posterior between our method (black line) and LVC (red dashed line) arises only due to the difference in the velocity correction between our method and LVC. In addition to calibration noise and peculiar velocity measurements, the main source of the error in the measurement of H_0 is due to the degeneracy between the inclination angle i and the distance d_L (Abbott et al. 2017a). This acts as a limiting factor for the measurement of H_0 from GW170817, if there is no independent measurement of inclination angle. Critically, the addition of Virgo (Acernese et al. 2015) to the nearly co-aligned two LIGO detectors (Abramovici et al. 1992; Abbott et al. 2016) allowed for the improvement in the sky localization of the GW source and a possibility of improving the measurement of the inclination angle.

A further improvement in the measurement of H_0 is possible if the uncertainty in the inclination angle i can be reduced. A recent study has used the observed data of the electromagnetic counterpart to GW170817, the superluminal motion measured by the VLBI (Very Large Baseline Interferometry) observations (Mooley et al. 2018a) and the afterglow light curve data (e.g., Mooley et al. (2018b)), to constrain the inclination angle of GW170817. Using the constraints on the inclination angle, Hotokezaka et al. (2019) obtained a revised value of H_0 . We implement our velocity field correction method for the combined measurement of GW+VLBI, by using a flat prior on the value of inclination angle between $0.25 \text{ rad} \leq i \left(\frac{d_L}{41 \text{ Mpc}}\right) \leq 0.45 \text{ rad}$. The revised H_0 by our method is shown in Figure 10 in blue color and is compared with the H_0 value from Hotokezaka et al. (2019) (shown by the magenta dashed line). The error in the measurement of H_0 from GW+VLBI (Hotokezaka et al. 2019) arises from several sources such as the GW data, the shape of the light curve, flux centroid motion, and the peculiar velocity. Our new estimate of the peculiar velocity improves the precision of the H_0 measurement with GW+VLBI from $70.3^{+5.3}_{-5.0}$ km s⁻¹ Mpc⁻¹ to $68.3^{+4.6}_{-4.5}$ km s⁻¹ Mpc⁻¹.

7. Conclusions and future prospects

Cosmology with gravitational waves is a newly emerging field carrying enormous potential to explore new aspects of the Universe and fundamental physics (Saltas et al. 2014; Lombriser & Taylor 2016; Lombriser & Lima 2017; Sakstein & Jain 2017; Baker et al. 2017; Nishizawa 2018; Belgacem et al. 2018a; Pardo et al. 2018; Abbott et al. 2019b; Belgacem et al. 2018b, 2019; Mukherjee et al. 2019a,b). One of such primary science goals is

⁶ RA and Dec respectively denote the right ascension and declination.

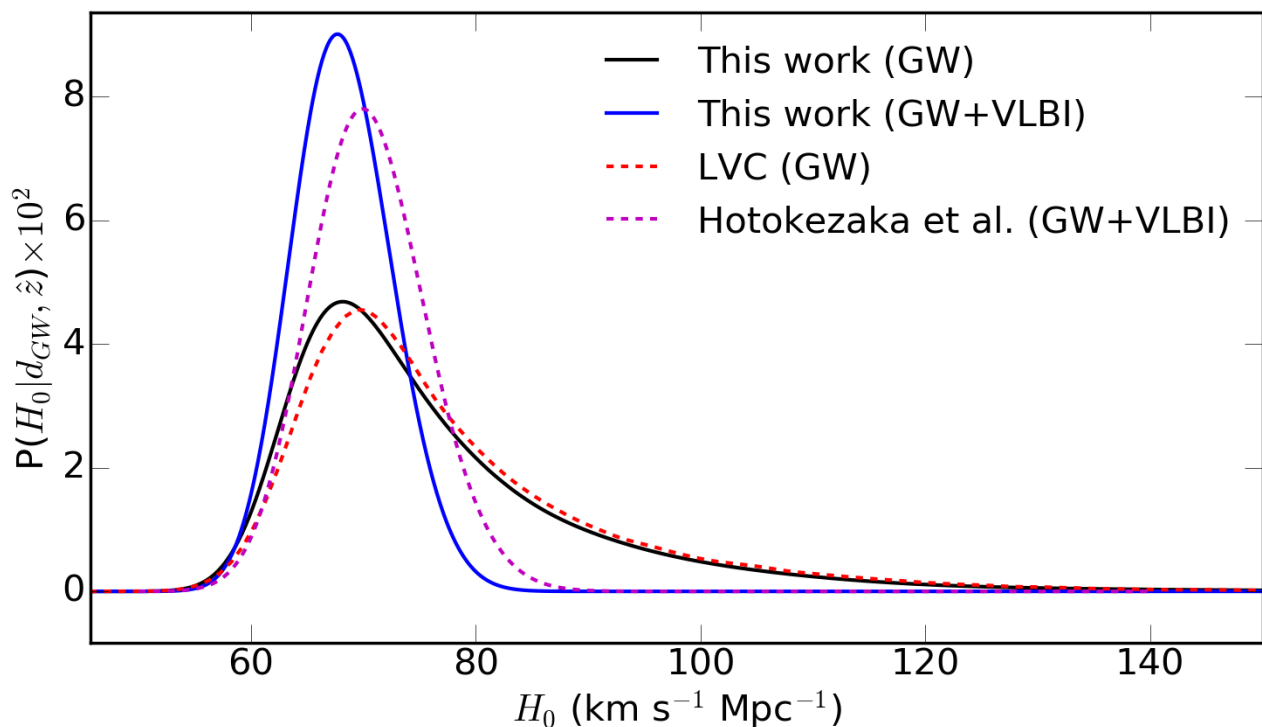


Fig. 10: The posterior of H_0 for GW170817 is obtained using the peculiar velocity correction by our method and is shown in black when we use the GW data and in blue when using the GW and VLBI data. We also show the H_0 measurement from the LIGO Scientific Collaboration and Virgo Collaboration (LVC) in dashed red line (Abbott et al. 2017a) and the magenta dashes presents the result from Hotokezaka et al. (2019) from hydrodynamics simulation jet using GW+VLBI observation .

the measurement of the Hubble constant from the GW sources if the redshift to the source can be identified from the electromagnetic counterpart or the cross-correlation with the galaxy surveys (Oguri 2016; Mukherjee & Wandelt 2018). With the current GW detectors such as Advanced LIGO (Abbott et al. 2016), and Advanced Virgo (Acernese et al. 2015), recent forecasts predict the ability to measure H_0 with an accuracy of less than 2% with about 50 BNS events (Chen et al. 2018; Feeney et al. 2019). To achieve such a precise estimation of H_0 , it is essential to accurately correct for the peculiar velocity of the hosts of GW sirens. This is particularly the case for very low redshift sources, which will have high signal-to-noise ratio and hence significantly contribute to the joint posteriors for ensembles of events. In addition, peculiar velocity corrections will be important for events with more favourable signal to noise in the Virgo or additional other detectors, as well as neutron star-black hole mergers (Nissanke et al. 2010; Vitale & Chen 2018). The absence of such a correction will affect both the accuracy and precision of the measurement of the value of H_0 . For a typical value of peculiar velocity of about $\sim 300 \text{ km s}^{-1}$ for a GW host at redshift $z = 0.01$, the contribution from peculiar velocity is comparable to the term related to the Hubble flow. The contribution becomes less (or more) severe at higher (or lower) redshift. As a result, we need to estimate the value of the peculiar velocity with sufficient accuracy in order to avoid any systematic bias and additional variance in the measurement of H_0 . Though averaging over a large GW samples can lead to an unbiased estimate of H_0 , the absence of a peculiar velocity correction will increase the error budget on H_0 due to the additional variance from the peculiar velocity contribution. In such a case, one needs a larger number of GW samples N_{gw} to beat the variance as $N_{gw}^{-1/2}$ (Nissanke et al. 2010; Nissanke

et al. 2013a; Chen et al. 2018; Feeney et al. 2019; Mortlock et al. 2018). Incorporating an accurate correction for the peculiar velocity of the host of GW sources, we can achieve faster and more economically both accurate, and precise measurements of H_0 .

In this paper, we use a statistical reconstruction method to correct the peculiar velocity of the host of the GW sources. The peculiar velocity for the host galaxy arises from the gravitational potential of the cosmic density field. We estimate the posterior of the peculiar velocity for both the linear and the non-linear component. The large scale velocity flow is estimated using the Bayesian framework called `borg`. The stochastic velocity dispersion of the source is obtained using a numerical fitting-form given in Eq. (6), by using the mass of the halo of the host. By combining the results from peculiar velocity estimate for each source, their redshifts, and the inferred luminosity distance from the GW data, we obtain a Bayesian inference of the value of H_0 according to the framework discussed around Eq. (7).

We implement our method on GW170817 (Abbott et al. 2017b) which is in the host NGC 4993 (Pan et al. 2017). The corresponding posterior distribution with the results from LVC (Abbott et al. 2017a) and GW+VLBI (Hotokezaka et al. 2019) are shown in Figure 10 by the solid line in black and blue color respectively. While our correction marginally reduces the maximum a posteriori value of H_0 to $68.3^{+4.6}_{-4.5} \text{ km s}^{-1} \text{ Mpc}^{-1}$ for GW+VLBI, it slightly disfavors very low values of $H_0 \lesssim 60 \text{ km s}^{-1} \text{ Mpc}^{-1}$ compared to the results from LVC. As we were preparing this manuscript for submission, an analysis appeared (Howlett & Davis 2019) that implemented an alternative velocity correction approach to the host of GW170817, and recovered a value of $H_0 = 64.8^{+7.3}_{-7.2} \text{ km s}^{-1} \text{ Mpc}^{-1}$. The mean value of H_0 differs from the values obtained in this work ($H_0 = 68.3^{+4.6}_{-4.5}$

$\text{km s}^{-1} \text{Mpc}^{-1}$) and also from the value obtained by Hotokezaka et al. (2019) ($H_0 = 70.3^{+5.3}_{-5.0} \text{ km s}^{-1} \text{Mpc}^{-1}$). However, the value by Howlett & Davis (2019) is consistent within the error-bars of both the estimations. Also another recent work (Nicolaou et al. 2020) has discussed the possible impact of peculiar velocity on the standard siren measurements, and has obtained a revised value of $H_0 = 68.6^{+14}_{-8.5} \text{ km s}^{-1} \text{Mpc}^{-1}$ for the event GW170817. Furthermore, a recent work by Boruah et al. (2020) also discusses the impact of line of sight marginalization for models derived using linear theory applied to spectroscopic data, calibrated with supernovae data, and velocity field derived from the distance data obtained from Tully-Fisher or Fundamental Plane methods.

The velocity correction is readily available for GW sources with electromagnetic counterparts (such as binary neutron stars, black hole neutron star) in the cosmic volumes covered by the 2M++ (Lavaux & Hudson 2011a; Jasche & Lavaux 2019) and the SDSS-III/BOSS surveys (Eisenstein et al. 2011; Dawson et al. 2013; Lavaux et al. 2019, see Figure 7). The 2M++ volume covers galactic latitudes $|b| > 10^\circ$ up to redshift $z \sim 0.05$; the SDSS-III/BOSS survey spans redshifts $z \sim 0.2 - 0.7$ for the sky areas ($0^\circ < \text{Dec} < 60^\circ$ and $120^\circ < \text{RA} < 240^\circ$) or ($0^\circ < \text{Dec} < 30^\circ$ and $|\text{RA}| < 30^\circ$). We expect that, within a year, our method will be available for the SDSS-IV/eBOSS survey (Dawson et al. 2016). In the long term, with the availability of the nearly full sky data sets jointly from the upcoming cosmology missions such as DESI (Dark Energy Spectroscopic Instrument, Aghamousa et al. 2016), and LSST (Large Synoptic Survey Telescope, LSST Science Collaboration et al. 2009), our algorithm will be available for most of the low redshift GW sources which will be observed by the currently planned network of ground-based GW detectors (Schutz 2011; Abbott et al. 2018).

Acknowledgements. SM would like to thank Emanuele Berti, Rahul Biswas, Stephen Feeney, Daniel Mortlock, Daniel Sclonic and Joseph Silk for fruitful discussions. SM and SMN would like to thank Hiranya Peiris and Will Farr for useful comments on the draft of the paper. The Flatiron Institute is supported by the Simons Foundation. SM is supported by the Lagrange postdoctoral Fellowship at Institut d’Astrophysique de Paris. The work of SM and BDW are also supported by the Labex ILP (reference ANR-10-LABX-63) part of the Idex SUPER, and received financial state aid managed by the Agence Nationale de la Recherche, as part of the programme Investissements d’avenir under the reference ANR-11-IDEX-0004-02. BDW thanks the CCPP at New York University for its hospitality while this work was completed. This work was supported by the ANR BIG4 project, grant ANR-16-CE23-0002 of the French Agence Nationale de la Recherche. SM and SMN are grateful for support from NWO VIDI and Projectruimte Grants of the Innovational Research Incentives Scheme (Vernieuwingsimpuls) financed by the Netherlands Organization for Scientific Research (NWO). FL acknowledges funding from the Imperial College London Research Fellowship Scheme. KH is supported by Lyman Spitzer Jr. Fellowship at Department of Astrophysical Sciences, Princeton University. This work was granted access to the HPC resources of CINES (Centre Informatique National de l’Enseignement Supérieur) under the allocation A0020410153 made by GENCI and has made use of the Horizon cluster hosted by the Institut d’Astrophysique de Paris in which the cosmological simulations were post-processed. We thank Stéphane Rouberol for running smoothly this cluster for us. This work is done within the Aquila Consortium⁷ We acknowledge the use of following packages in this analysis: Astropy (Astropy Collaboration et al. 2013, 2018), emcee: MCMC Hammer (Foreman-Mackey et al. 2013), IPython (Pérez & Granger 2007), Matplotlib (Hunter 2007), NumPy (van der Walt et al. 2011), and SciPy (Jones et al. 2001). The authors would like to thank the LIGO scientific collaboration and Virgo collaboration for providing the data for the event GW170817.

References

Abbott, B. P. et al. 2016, Phys. Rev., D93, 112004, [Addendum: Phys. Rev.D97,no.5,059901(2018)]

⁷ <https://www.aquila-consortium.org/>

- Abbott, B. P. et al. 2017a, Nature, 551, 85
 Abbott, B. P. et al. 2017b, Phys. Rev. Lett., 119, 161101
 Abbott, B. P. et al. 2018, Living Rev. Rel., 21, 3
 Abbott, B. P. et al. 2019a, Phys. Rev., X9, 011001
 Abbott, B. P. et al. 2019b, Phys. Rev. Lett., 123, 011102
 Abbott, T. M. C., Abdalla, F. B., Annis, J., et al. 2018, MNRAS, 480, 3879
 Abramovici, A., Althouse, W. E., Drever, R. W. P., et al. 1992, Science, 256, 325
 Acernese, F. et al. 2015, Class. Quant. Grav., 32, 024001
 Addison, G. E., Watts, D. J., Bennett, C. L., et al. 2018, ApJ, 853, 119
 Aghamousa, A. et al. 2016 [arXiv:1611.00036]
 Agrawal, P., Cyr-Racine, F.-Y., Pinner, D., & Randall, L. 2019 [arXiv:1904.01016]
 Anderson, L. et al. 2014, Mon. Not. Roy. Astron. Soc., 441, 24
 Astropy Collaboration, Price-Whelan, A. M., Sipőcz, B. M., et al. 2018, AJ, 156, 123
 Astropy Collaboration, Robitaille, T. P., Tollerud, E. J., et al. 2013, A&A, 558, A33
 Aubourg, E. et al. 2015, Phys. Rev., D92, 123516
 Baker, T., Bellini, E., Ferreira, P. G., et al. 2017, Phys. Rev. Lett., 119, 251301
 Barausse, E., Matarrese, S., & Riotto, A. 2005, Phys. Rev., D71, 063537
 Belgacem, E., Dirian, Y., Foffa, S., & Maggiore, M. 2018a, Phys. Rev., D97, 104066
 Belgacem, E., Dirian, Y., Foffa, S., & Maggiore, M. 2018b, Phys. Rev., D98, 023510
 Belgacem, E. et al. 2019, JCAP, 1907, 024
 Bennett, C. L. et al. 2013, ApJS, 208, 20
 Bernal, J. L., Verde, L., & Riess, A. G. 2016, JCAP, 1610, 019
 Bonvin, C., Durrer, R., & Gasparini, M. A. 2006, Phys. Rev., D73, 023523, [Erratum: Phys. Rev.D85,029901(2012)]
 Boruah, S. S., Hudson, M. J., & Lavaux, G. 2020 [arXiv:2010.01119]
 Branchini, E., Freudling, W., Da Costa, L. N., et al. 2001, MNRAS, 326, 1191
 Branchini, E., Teodoro, L., Frenk, C. S., et al. 1999, Monthly Notices of the Royal Astronomical Society, 308, 1
 Carrick, J., Turnbull, S. J., Lavaux, G., & Hudson, M. J. 2015, Mon. Not. Roy. Astron. Soc., 450, 317
 Chen, H.-Y., Fishbach, M., & Holz, D. E. 2018, Nature, 562, 545
 Chodorowski, M. J. & Cieliegielag, P. 2002, MNRAS, 331, 133
 Crook, A. C., Huchra, J. P., Martimbeau, N., et al. 2007, Astrophys. J., 655, 790
 Cuesta, A. J. et al. 2016, Mon. Not. Roy. Astron. Soc., 457, 1770
 Cutler, C. & Flanagan, E. E. 1994, Phys. Rev., D49, 2658
 Dalal, N., Holz, D. E., Hughes, S. A., & Jain, B. 2006, Phys. Rev., D74, 063006
 Davis, M., Nusser, A., Masters, K. L., et al. 2011, Monthly Notices of the Royal Astronomical Society, 413, 2906
 Davis, M., Nusser, A., & Willick, J. A. 1996, ApJ, 473, 22
 Dawson, K. S., Kneib, J.-P., Percival, W. J., et al. 2016, AJ, 151, 44
 Dawson, K. S., Schlegel, D. J., Ahn, C. P., et al. 2013, The Astronomical Journal, 145, 10
 Di Valentino, E., Melchiorri, A., & Mena, O. 2017, Phys. Rev. D, 96, 043503
 Ebrova, I. & Bilek, M. 2018 [arXiv:1801.01493]
 Eisenstein, D. J., Weinberg, D. H., Agol, E., et al. 2011, The Astronomical Journal, 142, 72
 Erdođdu, P., Lahav, O., Huchra, J. P., et al. 2006, MNRAS, 373, 45
 Fairhurst, S. 2009, New Journal of Physics, 11, 123006
 Fairhurst, S. 2011, Class. Quant. Grav., 28, 105021
 Feeney, S. M., Peiris, H. V., Williamson, A. R., et al. 2019, Phys. Rev. Lett., 122, 061105
 Foreman-Mackey, D., Hogg, D. W., Lang, D., & Goodman, J. 2013, PASP, 125, 306
 Freedman, W. L. et al. 2019 [arXiv:1907.05922]
 Hahn, O., Angulo, R. E., & Abel, T. 2015, MNRAS, 454, 3920
 Hawking, S. W. & Israel, W. 1987, Three hundred years of gravitation (Cambridge University Press)
 Hinshaw, G. et al. 2013, ApJS, 208, 19
 Holz, D. E. & Hughes, S. A. 2005, ApJ, 629, 15
 Hotokezaka, K., Nakar, E., Gottlieb, O., et al. 2019, Nature Astron. [arXiv:1806.10596]
 Howlett, C. & Davis, T. M. 2019 [arXiv:1909.00587]
 Hubble, E. 1929, Proceedings of the National Academy of Science, 15, 168
 Hudson, M. J. 1994, MNRAS, 266, 475
 Hudson, M. J., Smith, R. J., Lucey, J. R., & Branchini, E. 2004, MNRAS, 352, 61
 Hunter, J. D. 2007, Computing In Science & Engineering, 9, 90
 Jasche, J. & Lavaux, G. 2019, Astronomy & Astrophysics, 625, A64
 Jasche, J., Leclercq, F., & Wandelt, B. D. 2015, Journal of Cosmology and Astroparticle Physics, 2015, 036, arXiv:1409.6308
 Jasche, J. & Wandelt, B. D. 2013, Mon. Not. Roy. Astron. Soc., 432, 894
 Jee, I., Suyu, S., Komatsu, E., et al. 2019 [arXiv:1909.06712]
 Jennings, E. 2012, MNRAS, 427, L25
 Jennings, E., Baugh, C. M., & Pascoli, S. 2011, MNRAS, 410, 2081

- Jones, E., Oliphant, T., Peterson, P., et al. 2001, SciPy: Open source scientific tools for Python
- Kaiser, N., Efstathiou, G., Saunders, W., et al. 1991, MNRAS, 252, 1
- Knox, L. & Millea, M. 2019 [arXiv:1908.03663]
- Kolb, E. W., Matarrese, S., Notari, A., & Riotto, A. 2005, Phys. Rev., D71, 023524
- Kreisch, C. D., Cyr-Racine, F.-Y., & Doré, O. 2019 [arXiv:1902.00534]
- Lavaux, G. & Hudson, M. J. 2011a, MNRAS, 416, 2840
- Lavaux, G. & Hudson, M. J. 2011b, Monthly Notices of the Royal Astronomical Society, 416, 2840
- Lavaux, G. & Jasche, J. 2016, Mon. Not. Roy. Astron. Soc., 455, 3169
- Lavaux, G., Jasche, J., & Leclercq, F. 2019, submitted to MNRAS [arXiv:TBD]
- Leclercq, F., Jasche, J., Lavaux, G., Wandelt, B., & Percival, W. 2017, Journal of Cosmology and Astroparticle Physics, 2017, 049
- Leclercq, F., Jasche, J., & Wandelt, B. 2015, Journal of Cosmology and Astroparticle Physics, 2015, 15
- Lemaître, G. 1927, Annales de la Société Scientifique de Bruxelles, 47, 49
- Lemaître, G. 1931, MNRAS, 91, 483
- Lin, M.-X., Benevento, G., Hu, W., & Raveri, M. 2019 [arXiv:1905.12618]
- Lombriser, L. & Lima, N. A. 2017, Phys. Lett., B765, 382
- Lombriser, L. & Taylor, A. 2016, JCAP, 1603, 031
- LSST Science Collaboration, Abell, P. A., Allison, J., et al. 2009, arXiv e-prints, arXiv:0912.0201
- Ma, Y.-Z., Branchini, E., & Scott, D. 2012, MNRAS, 425, 2880
- Macaulay, E. et al. 2019, Mon. Not. Roy. Astron. Soc., 486, 2184
- Maggiore, M. 2008, Gravitational Waves: Volume 1: Theory and Experiments, Gravitational Waves (OUP Oxford)
- Mooley, K. P., Deller, A. T., Gottlieb, O., et al. 2018a, Nature, 561, 355
- Mooley, K. P., Frail, D. A., Dobie, D., et al. 2018b, ApJL, 868, L11
- Mortlock, D. J., Feeney, S. M., Peiris, H. V., Williamson, A. R., & Nissanke, S. M. 2018 [arXiv:1811.11723]
- Mukherjee, S. & Wandelt, B. D. 2018, arXiv:1808.06615 [arXiv:1808.06615]
- Mukherjee, S., Wandelt, B. D., & Silk, J. 2019a [arXiv:1908.08950]
- Mukherjee, S., Wandelt, B. D., & Silk, J. 2019b [arXiv:1908.08951]
- Neyrinck, M. C., Aragón-Calvo, M. A., Jeong, D., & Wang, X. 2014, Mon. Not. Roy. Astron. Soc., 441, 646
- Nicolaou, C., Lahav, O., Lemos, P., Hartley, W., & Braden, J. 2020, Mon. Not. Roy. Astron. Soc., 495, 90
- Nishizawa, A. 2018, Phys. Rev., D97, 104037
- Nissanke, S., Holz, D. E., Dalal, N., et al. 2013a [arXiv:1307.2638]
- Nissanke, S., Holz, D. E., Hughes, S. A., Dalal, N., & Sievers, J. L. 2010, ApJ, 725, 496
- Nissanke, S., Kasliwal, M., & Georgieva, A. 2013b, Astrophys. J., 767, 124
- Nissanke, S., Sievers, J., Dalal, N., & Holz, D. 2011, ApJ, 739, 99
- Nusser, A., Da Costa, L. N., Branchini, E., et al. 2001, Monthly Notices of the Royal Astronomical Society, 320, L21
- Oguri, M. 2016, Phys. Rev. D, 93, 083511
- Pan, Y. C. et al. 2017, ApJ, 848, L30
- Pardo, K., Fishbach, M., Holz, D. E., & Spergel, D. N. 2018, JCAP, 1807, 048
- Pérez, F. & Granger, B. E. 2007, Computing in Science and Engineering, 9, 21
- Pike, R. W. & Hudson, M. J. 2005, ApJ, 635, 11
- Planck collaboration. 2014, Astron. Astrophys., 571, A16
- Planck collaboration. 2016, Astron. Astrophys., 594, A13
- Planck collaboration. 2018 [arXiv:1807.06209]
- Poisson, E. & Will, C. M. 1995, Phys. Rev., D52, 848
- Poulin, V., Smith, T. L., Karwal, T., & Kamionkowski, M. 2019, Phys. Rev. Lett., 122, 221301
- Radburn-Smith, D. J., Lucey, J. R., & Hudson, M. J. 2004, Monthly Notices of the Royal Astronomical Society, 355, 1378
- Reid, M. J., Braatz, J. A., Condon, J. J., et al. 2009, ApJ, 695, 287
- Riess, A. G., Casertano, S., Yuan, W., Macri, L. M., & Scolnic, D. 2019, ApJ, 876, 85
- Sakstein, J. & Jain, B. 2017, Phys. Rev. Lett., 119, 251303
- Saltas, I. D., Sawicki, I., Amendola, L., & Kunz, M. 2014, Phys. Rev. Lett., 113, 191101
- Sasaki, M. 1987, MNRAS, 228, 653
- Saunders, W., Oliver, S., Keeble, O., et al. 2000, in Astronomical Society of the Pacific Conference Series, Vol. 201, Cosmic Flows Workshop, ed. S. Courteau & J. Willick, 223
- Schutz, B. F. 1986, Nature, 323, 310
- Schutz, B. F. 2011, Classical and Quantum Gravity, 28, 125023
- Schutz, B. F. 2011, Class. Quant. Grav., 28, 125023
- Soccimarro, R. 2004, Phys.Rev.D, 70, 083007
- Seto, N. & Kyutoku, K. 2018, MNRAS, 475, 4133
- Shaya, E. J., Tully, R. B., & Pierce, M. J. 1992, ApJ, 391, 16
- Sheth, R. K. & Diaferio, A. 2001, MNRAS, 322, 901
- Springel, V. 2005, Monthly Notices of the Royal Astronomical Society, 364, 1105
- Springob, C. M., Magoulas, C., Colless, M., et al. 2014, Mon. Not. Roy. Astron. Soc., 445, 2677
- Springob, C. M., Masters, K. L., Haynes, M. P., Giovanelli, R., & Marinoni, C. 2007, ApJS, 172, 599
- Turnbull, S. J., Hudson, M. J., Feldman, H. A., et al. 2012a, MNRAS, 420, 447
- Turnbull, S. J., Hudson, M. J., Feldman, H. A., et al. 2012b, MNRAS, 420, 447
- van der Walt, S., Colbert, S. C., & Varoquaux, G. 2011, Computing in Science and Engineering, 13, 22
- Veitch, J., Mandel, I., Aylott, B., et al. 2012, Phys.Rev.D, 85, 104045
- Verde, L., Protopapas, P., & Jimenez, R. 2013, Phys. Dark Univ., 2, 166
- Verde, L., Treu, T., & Riess, A. G. 2019, in Tensions between the Early and the Late Universe
- Vitale, S. & Chen, H.-Y. 2018, Phys. Rev. Lett., 121, 021303
- Wong, K. C. et al. 2019 [arXiv:1907.04869]
- Yuan, W., Riess, A. G., Macri, L. M., Casertano, S., & Scolnic, D. 2019 [arXiv:1908.00993]